

Zener tunneling isospin Hall effect in HgTe quantum wells and graphene multilayers

M. Lasia, E. Prada, and L. Brey

Instituto de Ciencia de Materiales de Madrid, (CSIC), Cantoblanco, E-28049 Madrid, Spain

(Received 24 April 2012; published 27 June 2012)

A Zener diode is a paradigmatic device in semiconductor-based electronics that consists of a p - n junction where an external electric field induces a switching behavior in the current-voltage characteristics. We study Zener tunneling in HgTe quantum wells and graphene multilayers. We find that the tunneling transition probability depends asymmetrically on the parallel momentum of the carriers to the barrier. In HgTe quantum wells the asymmetry is the opposite for each spin, whereas for graphene multilayers it is the opposite for each valley degree of freedom. In both cases, a spin/valley current flowing in the perpendicular direction to the applied field is produced. We relate the origin of this *Zener tunneling spin/valley Hall effect* to the Berry phase acquired by the carriers when they are adiabatically reflected from the gapped region.

DOI: [10.1103/PhysRevB.85.245320](https://doi.org/10.1103/PhysRevB.85.245320)

PACS number(s): 73.40.Gk, 72.80.Vp, 85.75.-d, 03.65.Vf

I. INTRODUCTION

A large class of semiconductor devices is based on quantum mechanical tunneling of carriers through potential barriers. This is the case of the *Zener diode*, which consists of a p - n junction where a strong enough electric field induces interband transitions from the valence band of the p -type material to the conduction band of the n -doped material [see Fig. 1(a)]. The tunneling amplitude is highly nonlinear in the applied field, and the tunneling current shows a breakdown-type behavior in the current-voltage (I - V) characteristics. The nonlinearity of the Zener tunneling makes this device very useful for semiconductor-based electronics.¹ Interband tunneling has been studied extensively in parabolic band-gap semiconductors; it is a paradigmatic example of nonadiabatic transitions, and it is known as the Landau-Zener tunneling.^{2,3} The most used model for studying the interband tunneling in parabolic semiconductors is a two-level system described by a Dirac-like Hamiltonian with a mass term^{3–5} [see Fig. 1(b)]. In this kind of material, the spin of the carriers typically plays no role.

In this paper we are interested in analyzing Zener tunneling physics in systems in which there is a correlation between the carrier's spin (or an equivalent degree of freedom) and its direction of motion i.e., systems in which *chirality* plays a role. In particular, we analyze two types of materials, HgTe quantum wells and carbon-based planar heterostructures. These materials have in common that they can be described by 2×2 Hamiltonians and, therefore, it is possible to map the tunneling problem to the evolution of a two-level system.⁶

In the first case, HgTe quantum wells, we find that the Zener tunneling depends asymmetrically on the parallel momentum of the carriers to the barrier, and this asymmetry is the opposite for each spin. We call this phenomenon *Zener tunneling spin Hall effect*. In these quantum wells the central region is an inverted band-gap semiconductor, such as HgTe, whose intrinsic strong spin-orbit coupling induces an inversion of the normal band progression of typical semiconductors, like the one used for the barrier material (e.g., CdTe). This kind of material has come to the spotlight recently because, depending on the width of the central region, the system can undergo a quantum phase transition and become a topological insulator.^{7–9} A topological insulator is a novel quantum state

of matter that has metallic surface states inside the bulk energy gap.^{10–12}

In the second case, graphene multilayers, we find that the Zener tunneling is also asymmetric with respect to the parallel momentum (except for monolayer), but the asymmetry changes for each carrier's valley index (instead of real spin). We call this phenomenon *Zener tunneling valley Hall effect*. Graphitic systems are also of great interest in condensed matter physics since it became possible to isolate monolayers, bilayers and in general multilayers of graphene.^{13–15} p - n junctions of graphene have been created by gating locally these layers and the transport properties of these heterostructures have been studied theoretically and experimentally.^{16–26} In particular, in bilayer graphene it is possible to open a gap in the spectrum by applying a voltage difference between the layers, and Zener tunneling is expected to occur. Actually, it has recently been predicted that the I - V characteristics in bilayer graphene p - n junctions present, on top of the nonlinear Zener signal, some N-shaped branches with negative differential conductivity.²⁷

In both types of materials, the low-energy Hamiltonian can be expressed in terms of a *pseudospin vector* that multiplies the vector of Pauli matrices. In a tunneling process, the pseudospin vector undergoes a certain trajectory in the Bloch sphere and the carrier's wave function may acquire a Berry phase. We relate the Zener transition asymmetry with the spin/valley-dependent Berry phase that the carriers acquire when they are adiabatically reflected from the gapped region.

The paper is organized in the following way: In Sec. II we define the Hamiltonians that govern the properties of HgTe quantum wells and graphene multilayers. In Sec. III we map the tunneling problem to the time evolution of a two-level system and show numerical results for the different Hamiltonians. In Sec. IV we derive analytical expressions for the tunneling transition in the sudden and adiabatic approximations. In Sec. V the asymmetry of the tunneling amplitude as a function of the momentum parallel to the barrier is explained in terms of the Berry phases that the carriers acquire upon reflection from the barrier. In Sec. VI we show the I - V characteristic curves for the HgTe quantum well and multilayer graphene Zener diodes. We finish the paper in Sec. VII with a summary of our results.

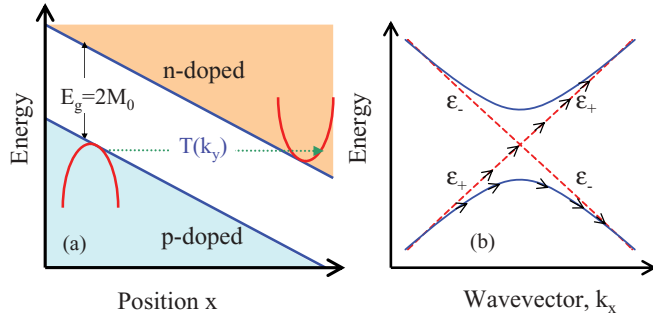


FIG. 1. (Color online) (a) Schematic representation of a tunneling process in a Zener diode in the uniform electric field approximation. $T(k_y)$ represents the transition probability of a quasiparticle with momentum k_y from the p -doped valence band to the n -doped conduction band. (b) Wave-vector-energy scheme for the two-band model. The diabatic (adiabatic) energy levels are plotted in dashed red (solid blue) lines. Near the anticrossing region a diabatic ϵ_+ state can tunnel to the diabatic state ϵ_- .

II. HAMILTONIANS

A. HgTe quantum wells

We study a HgTe quantum well confined by CdTe barriers. In bulk, and due to the strong spin-orbit coupling, HgTe is a zero gap semiconductor. When confined, HgTe is a normal band insulator for well thickness narrower than 63 \AA and becomes a topological insulator for larger widths.⁹ For HgTe quantum wells grown in the (100) direction, the z component of the spin is conserved. Near the band gap there are four relevant bands: the $E1$ bands that consist of the two spin states of the s orbital, and the two spin states of the $HH1$ bands which are a linear combination of the p_x and p_y orbitals. The low-energy effective Hamiltonian for the two spin orientations, $s_z = \pm 1$, reads

$$H_{s_z}(\mathbf{k}) = \epsilon(k)\underline{I} + M(k)\sigma_z + A(k_y\sigma_y + s_z k_x\sigma_x), \quad (1)$$

where $\mathbf{k} = (k_x, k_y)$ is the in-plane wave vector of the carriers, $k = |\mathbf{k}|$, $\epsilon(k) = C - D(k_x^2 + k_y^2)$, $M(k) = M_0 + B(k_x^2 + k_y^2)$, σ_x , σ_y , and σ_z are the Pauli matrices, and \underline{I} is the identity. $E_g = 2M_0$ is the band gap and A - D are parameters fitting the HgTe quantum wells.²⁸ The product M_0B determines the character of the insulator. For $M_0B > 0$ the system is a normal insulator, whereas for $M_0B < 0$ a band inversion occurs and the system becomes a topological insulator. The p - n structure of the Zener diode is described by adding to the Hamiltonian the appropriate scalar external potential of the form $V(x)\underline{I}$.

B. Multilayer graphene

In graphene and its multilayers, the low-energy properties occur near two nonequivalent valleys \mathbf{K} and \mathbf{K}' and the motion of the carriers depends on the valley where they reside. The role that the spin plays in HgTe quantum wells is played here by the valley index, $\tau_z \pm 1$. Recently, it has been predicted that spin-orbit coupling in graphene opens a gap and the system could become a topological insulator.^{29,30} However, this gap is very small and the occurrence of the quantized spin Hall effect would be observed at extremely low temperatures and in extremely clean samples.³¹ Thus, neglecting spin-orbit

coupling, the low-energy properties of N -layer ABC -stacked multilayers are described, in general, by the Hamiltonian,^{32,33}

$$H_{\tau_z}^N = \frac{(v_F p)^N}{(-\gamma_1)^{N-1}} [\cos(N\phi_p)\sigma_x + \sin(N\phi_p)\sigma_y] + M_0\sigma_z. \quad (2)$$

Here the notation is $\cos\phi_p = p_x/p$ and $\sin\phi_p = \tau_z p_y/p$, where $p_{x,y} = \hbar k_{x,y}$. In the previous expression the Pauli matrices act on the external layers for $N \geq 1$ and on atoms A and B of the unit cell in monolayer graphene. $v_F \sim 1 \times 10^6 \text{ ms}^{-1}$ is the velocity of the carriers in monolayer graphene³² and $\gamma_1 \sim 0.3 \text{ eV}$ is the strongest direct interlayer hopping.³⁴ The last term in Eq. (2) opens a gap in the spectrum. In multilayer graphene this term represents an externally controlled potential shift in the chemical potential between the external layers. In monolayer graphene, though, it is not possible to open a gap experimentally, but we are going to study this possibility for the sake of completeness. Note, however, that at the surface of a three-dimensional (3D) topological insulator there will exit a Dirac-like electron system^{35,36} that, doped with magnetic impurities, will develop a gap. The band structure of this surface state is governed by the same 2×2 Hamiltonian than monolayer graphene, but with the σ matrices referring to the real electron spin.

As in the HgTe case, we describe the p - n structure of the Zener diode adding a scalar term, $V(x)\underline{I}$, to the Hamiltonian of Eq. (2).

III. CONSTANT FIELD AND THE TWO-LEVEL SYSTEM

In this work we describe Zener tunneling in the uniform electric field model, $V(x) = -Fx$ [see Fig. 1(a)]. In this approximation, it is possible to get the transmission across the p - n junction by mapping the problem into the evolution of a two-level system.^{4,27} The key is that for a uniform electric field, F , applied in the \hat{x} direction, the problem can be simplified if we use the momentum representation, $x = i\partial_{k_x}$. With it, the Schrödinger equation corresponding to Eqs. (1) and (2) becomes

$$iF \frac{\partial \psi_s}{\partial k_x} = [H_s(\mathbf{k}) - E]\psi_s, \quad (3)$$

where E is the energy and the index s stands for the spin or the valley index, depending on the system at hand. For each index, $s = \pm 1$, this equation is identical to the Bloch equation describing the dynamics of a spin-1/2 particle in the presence of a magnetic field, with the wave vector in the x direction playing the role of time. In the uniform electric field model, the term $[\epsilon(k) - E]\underline{I}$ for HgTe quantum wells in Eq. (3), or equivalently the term $E\underline{I}$ for multilayers, does not contribute to the interband transition and we drop it.

In the limit $k_x \rightarrow \pm\infty$ the eigenvalues of H_s are also eigenstates of σ_v , being $v = x$ for multilayer graphene and $v = z$ for HgTe quantum wells. Starting at $k_x \rightarrow -\infty$ from the low-energy eigenvector (with eigenvalue $\sigma_v = -1$) and tuning k_x from $-\infty$ to $+\infty$, the two-level system traverses a level anticrossing.⁶ Valence to conduction interband transitions are described by the process in which a state that at $k_x = -\infty$ has negative energy evolves into a state that at $k_x = +\infty$ has positive energy. We have solved numerically Eq. (3) in an interval $k_{x,\min} < k_x < k_{x,\max}$ such that, at $k_{x,\max}$ and $k_{x,\min}$, the

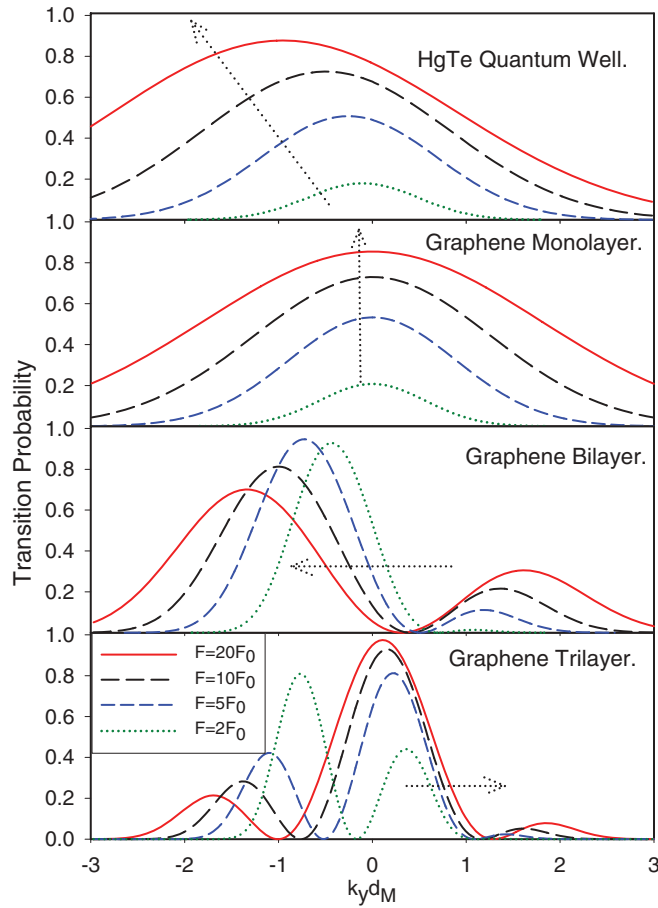


FIG. 2. (Color online) Zener tunneling in the constant field model as a function of the parallel momentum of the incident particle for HgTe quantum wells and multilayer graphene. The results correspond to spin/valley $s = 1$ (for $s = -1$ equivalent results are obtained, but specularly reflected with respect to $k_y = 0$). The direction of the arrows indicate the evolution of the curves when increasing the electric field.

eigenvalues of σ_v are ± 1 . From the evolution of Eq. (3) we obtain the wave function at $k_{x,\max}$ and from the square of its projection on the state with $\sigma_v = 1$ we obtain the interband transition probability.

In Fig. 2 we plot the Zener transition probability $T(k_y, s = 1, F)$ as a function of the wave vector k_y of the incident particle for a HgTe quantum well and for monolayer, bilayer, and trilayer graphene. We plot the transition probability for several values of the electric field, $F = 2, 5, 10$, and $20F_0$, with $F_0 \equiv M_0/d_M$. Here F_0 and d_M are the electric field and length characteristic scales set by the gap of the insulator: $d_M = A/M_0$ for HgTe quantum wells and $d_M = \hbar v_F (\frac{1}{M_0} \frac{1}{\gamma_1^{N-1}})^{1/N}$ for multilayer graphene.

The symmetry of the Hamiltonian dictates that $T(k_y, s, F) = T(-k_y, -s, F)$. Except for monolayer graphene, the transition probability has a maximum at a finite value of k_y that depends on the sign of s . As a result, carriers with positive spin/isospin are mainly deflected towards one \hat{y} direction when tunneling, whereas those with negative spin/isospin are deflected in the opposite direction. The overall transition probability increases with the applied

electric field (see Fig. 2). At small fields the spatial extension of the forbidden region becomes very large and the Zener tunneling amplitude goes to zero abruptly when $F \rightarrow 0$. This is the origin of the switching behavior of the Zener diodes. For moderate applied electric fields the asymmetry in the angle of incidence also increases with the field.

IV. SUDDEN AND ADIABATIC APPROXIMATIONS

In order to shed some light on our numerical results, we have solved Eq. (3) analytically in the limit of small parallel momentum k_y and large electric field. The analytical calculations expand the solution of the Hamiltonian in a *diabatic* or in an *adiabatic* basis [see Fig. 1(b)]. The first case is suitable for an unperturbed Hamiltonian that can be diagonalized in a diabatic basis, where the carriers evolve with probability one from the valence to the conduction band. We then calculate the first correction to perfect transmission in the sudden approximation, treating the rest of the Hamiltonian in first-order perturbation theory. When the Hamiltonian is such that the tunneling transmission from the valence to the conduction band is very small, it is more convenient to use the adiabatic basis as the unperturbed one. In the adiabatic basis the carriers are completely reflected at the barrier, and the tunneling probability can be obtained as first-order perturbation to the adiabatic Hamiltonian.

The Hamiltonians of the systems we are studying can be written in the form,

$$H = \varepsilon(\mathbf{k}) \vec{h}(\mathbf{k}) \cdot \vec{\sigma}. \quad (4)$$

This equation defines a wave-vector-dependent unitary pseudospin vector $\vec{h}(\mathbf{k})$. From the form of this Hamiltonian, the expectation value of the vector of σ matrices is either parallel, in the conduction band, or antiparallel, in the valence band, to the pseudospin. In the absence of gap, $M_0 = 0$, carriers approaching perpendicularly to the barrier, $k_y = 0$, should conserve the pseudospin. This is in agreement with the Klein paradox, which implies perfect transmission for gapless monolayer and trilayer graphene and perfect reflection for gapless bilayer graphene.¹⁶ This conservation of the pseudospin at $k_y = 0$ for massless Hamiltonians would help us to choose a diabatic or adiabatic basis as the starting point in perturbation theory.

A. HgTe quantum wells, diabatic basis, and sudden approximation

In HgTe quantum wells, the pseudospin has the form,

$$\vec{h}^{HgTe} = (Ak_x, Ak_y s_z, M_0 + Bk^2) / \sqrt{(M_0 + Bk^2)^2 + A^2 k^2}. \quad (5)$$

For $M_0 = 0$ and $B = 0$, the pseudospin takes the form $(k_x, k_y s_z, 0)/|k|$, and the eigenfunctions of the Hamiltonian of Eq. (1) are chiral. In this limit, the Klein paradox dictates¹⁶ that the tunneling amplitude at $k_y = 0$ is unity. For finite values of M_0 and B , the Klein paradox does not apply exactly, but the transmission probability at large electric fields and small values of M_0 and k_y is close to unity. Therefore, it is convenient to work in the diabatic basis.

In the natural units of the problem, $x \equiv k_x d_M$, $y \equiv k_y d_M$, $\mathcal{E} \equiv F/F_0$, and $\tilde{B} \equiv B/(M_0 d_M^2)$, the Hamiltonian is written as

$$i \frac{\partial}{\partial x} \psi \equiv (H_0 + \tilde{V})\psi, \text{ with} \quad (6)$$

$$H_0 = \frac{1}{\mathcal{E}} \begin{pmatrix} \tilde{B}x^2 & xs_z \\ xs_z & -\tilde{B}x^2 \end{pmatrix}, \quad \tilde{V} = \frac{1}{\mathcal{E}} \begin{pmatrix} 1 + \tilde{B}y^2 & -iy \\ iy & -1 - \tilde{B}y^2 \end{pmatrix}.$$

The eigenvectors of H_0 define the diabatic basis, with eigenvalues $\varepsilon_{\pm}(x) = \pm \frac{x}{\mathcal{E}} \sqrt{1 + \tilde{B}^2 x^2}$ [see Fig. 1(b)]. We represent the corresponding wave function in the diabatic basis as

$$\psi(x) = C_-(x)e^{-i\omega(x)}|-\rangle + C_+(x)e^{+i\omega(x)}|+\rangle, \quad (7)$$

where $H_0|\pm\rangle = \varepsilon_{\pm}|\pm\rangle$ and $\omega(x) = \int^x \varepsilon_+(x')dx'$. We define the transmission t and reflection amplitude r as follows: Assuming that $C_-(-\infty) = 0$ and $C_+(-\infty) = 1$, then $r = C_-(-\infty)$ and $t = C_+(\infty)$. Plugging the wave function, Eq. (7), into the Hamiltonian of Eq. (6), we get

$$\partial_x C_{\pm} = \pm \frac{i}{\mathcal{E}} T_0 C_{\pm} - \frac{i}{\mathcal{E}} T_{\pm} C_{\mp}, \quad \text{where} \quad (8)$$

$$T_0 = (1 + \tilde{B}y^2) \frac{\tilde{B}x^2}{\sqrt{x^2 + \tilde{B}^2 x^4}} \quad \text{and}$$

$$T_{\pm} = \mp e^{\mp 2i\phi(x)} \left(s_z x \frac{1 + \tilde{B}y^2}{\sqrt{x^2 + \tilde{B}^2 x^4}} + iy + i\mathcal{E}s_z \frac{\tilde{B}/2}{1 + \tilde{B}x^2} \right). \quad (9)$$

The amplitudes r and t are obtained from the asymptotic solution of Eq. (8) with the appropriate boundary conditions. For large values of \mathcal{E} it is possible to get an analytical expression for the transition. To lowest order in $1/\mathcal{E}$, the asymptotic form of C_- is obtained by substituting $C_+(x) = 1$ in Eq. (8),

$$C_-(\infty) = -\frac{i}{\mathcal{E}} \int_{-\infty}^{+\infty} T_- dx. \quad (10)$$

For small values of $\tilde{B}^2 \mathcal{E}$ this integral can be evaluated using the steepest descent method. From it we obtain the interband transition probability,

$$T(y, s_z) = 1 - |r|^2 \simeq 1 - \frac{\pi}{\mathcal{E}} \left(\left[1 + \tilde{B}y^2 + \frac{\tilde{B}^3 \mathcal{E}^2}{4} \right]^2 + \left[y + \frac{\mathcal{E}\tilde{B}}{2} s_z \left(1 - \frac{\tilde{B}}{2} \right) \right]^2 \right). \quad (11)$$

Recovering previous units, the maximum of the transition probability to lowest order in FB^2 occurs at a wave vector,

$$k_y^M = -s_z \frac{FB}{A^2} \left(1 - \frac{5}{2} \frac{B}{A^2} M_0 \right), \quad (12)$$

being the maximum transition probability,

$$T_{\max} = 1 - \frac{\pi}{F} \frac{M_0^2}{A}. \quad (13)$$

In Fig. 3 we compare the transmission at $k_y = 0$ obtained numerically from Eq. (3) with the one obtained from Eq. (11). The quality of the approximation is good, especially for strong

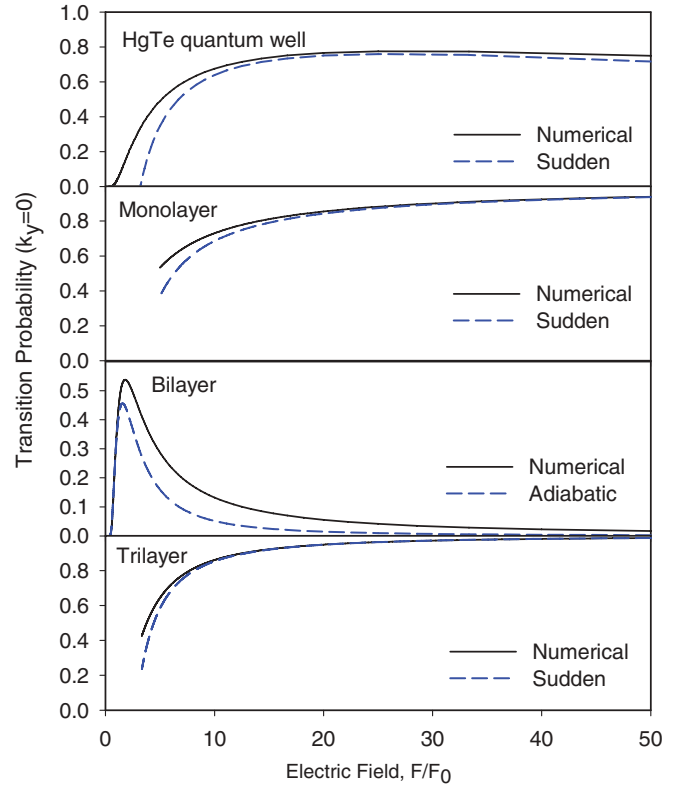


FIG. 3. (Color online) Comparison of the transmission probability at $k_y = 0$ obtained by solving numerically Eq. (3) with the analytical result obtained in first-order perturbation theory: Equation (11) for HgTe quantum wells, Eq. (19) for graphene, Eq. (28) for bilayer graphene, and Eq. (35) for trilayer graphene.

electric fields. Equations (12) and (13) explain qualitatively much of the results presented in the first panel of Fig. 2: (i) For each spin orientation the transition probability is asymmetric with respect to k_y , (ii) the asymmetry increases with the field, (iii) the sign of k_y^M depends on the product $s_z B$ (note that when $B = 0$ there is no spin Hall effect), (iv) the asymmetry is present either for $M_0 B > 0$ or $M_0 B < 0$ (i.e., irrespective of whether the quantum well is in the trivial or in the topological phase), and (v) the overall transition increases with the electric field. Moreover, Eqs. (12) and (13) describe quantitatively the results in the case of large F . For example, for $F/F_0 = 10$ we get $T_{\max} = 0.69$ and $k_y^M = 0.45$, results that are in rather good agreement with the numerical ones presented in Fig. 2.

A spin-dependent transmission has been also predicted to occur at the interface between a HgTe quantum well and a metal.³⁷ In this case the asymmetry is related to localized states at the interface.

B. Monolayer graphene, diabatic basis, and sudden approximation

The pseudospin vector for graphene has the form,

$$\vec{h}^m = (v_F p_x, v_F \tau_z p_y, M_0) / \sqrt{M_0^2 + v_F^2 p^2}, \quad (14)$$

and for gapless monolayer graphene the Klein paradox applies exactly. Therefore, in order to study the tunneling when $M_0 \neq 0$, it is convenient to work in the diabatic basis and, using

natural units as before, we write the Bloch-like equation as

$$i \frac{\partial}{\partial x} \psi = \left[\frac{1}{\mathcal{E}} \begin{pmatrix} 0 & x \\ x & 0 \end{pmatrix} + \frac{1}{\mathcal{E}} \begin{pmatrix} 1 & -iy\tau_z \\ iy\tau_z & -1 \end{pmatrix} \right] \psi. \quad (15)$$

Note that in the reduced units, $\hbar v_F$ plays the same role as A . The eigenvalues of the first term of Eq. (15) define the diabatic basis. Using this basis, the wave function takes the form,

$$\psi(x) = C_-(x) \frac{1}{\sqrt{2}} \begin{pmatrix} 1 \\ -1 \end{pmatrix} e^{i \frac{x^2}{2\mathcal{E}}} + C_+(x) \frac{1}{\sqrt{2}} \begin{pmatrix} 1 \\ 1 \end{pmatrix} e^{-i \frac{x^2}{2\mathcal{E}}}, \quad (16)$$

and the coefficients C_- and C_+ satisfy

$$\partial_x C_{\pm} = -\frac{i}{\mathcal{E}} (1 - iy\tau_z) e^{i \frac{x^2}{2\mathcal{E}}} C_{\pm}. \quad (17)$$

The reflection amplitude in the sudden approximation, valid in the $\mathcal{E} \rightarrow \infty$ limit, is then

$$r \simeq -\frac{i}{\mathcal{E}} (1 - iy\tau_z) \int_{-\infty}^{\infty} e^{i \frac{x^2}{2\mathcal{E}}} dx, \quad (18)$$

being the transition probability, in the original units,

$$T(k_y) = 1 - \frac{\pi}{F \hbar v_F} (M_0^2 + \hbar^2 k_y^2 v_F^2). \quad (19)$$

In agreement with the numerical results, we get that the transition probability is symmetric in k_y and independent on the isospin τ_z (see Fig. 2). Note that, for monolayer graphene, the transition probability can be obtained exactly,^{4,19}

$$T(k_y) = e^{-\frac{\pi}{F \hbar v_F} (M_0^2 + \hbar^2 k_y^2 v_F^2)}, \quad (20)$$

and Eq. (19) corresponds to the first term in the $1/F$ expansion. Figure 3, second panel, illustrates the quality of the sudden approximation at large values of the electric field.

C. Bilayer graphene and the adiabatic approximation

For bilayer graphene, the pseudospin has the form,

$$\vec{h}^b = \left(\frac{v_F^2}{\gamma_1} (p_x^2 - p_y^2), \frac{v_F^2}{\gamma_1} 2p_x p_y \tau_z, M_0 \right) / \sqrt{M_0^2 + \frac{v_F^4}{\gamma_1^2} p^4}. \quad (21)$$

Gapless bilayer graphene, $M_0 = 0$, is also chiral, and the pseudospin is $(k_x^2 - k_y^2, 2k_x k_y \tau_z, 0)/k^2$. Holes impinging perpendicularly to the barrier from the left have opposite pseudospin than electrons moving to the right, and the same pseudospin as holes reflecting from the barrier. Therefore, the tunneling probability for $M_0 = 0$ and $k_y = 0$ is null. When $M_0 \neq 0$, the transition probability at $k_y = 0$ is still small (see Fig. 2), and it is thus more appropriate to work in the adiabatic basis.

The Bloch equation for bilayer graphene has the form,

$$-i\mathcal{E} \frac{\partial}{\partial x} \psi = \begin{pmatrix} 1 & (x - iy\tau_z)^2 \\ (x + iy\tau_z)^2 \tau_z & -1 \end{pmatrix} \psi = H_B \psi, \quad (22)$$

where now $\mathcal{E} = \frac{\hbar v_F}{M_0} \frac{F}{\sqrt{M_0 \gamma_1}}$.

The Hamiltonian H_B in Eq. (22) defines the adiabatic basis with eigenvalues $\varepsilon(x, y) = \pm \sqrt{1 + (x^2 + y^2)^2}$ and eigenfunc-

tions,

$$\psi_- = \begin{pmatrix} -\sin(\theta/2) \\ \cos(\theta/2)e^{i\phi} \end{pmatrix} \text{ and } \psi_+ = \begin{pmatrix} \cos(\theta/2) \\ -\sin(\theta/2)e^{i\phi} \end{pmatrix}, \quad (23)$$

where $\cos(\theta) = 1/|\varepsilon|$ and $\phi = \tan^{-1}(\frac{-2xy}{x^2 - y^2})$. In order to solve Eq. (22) we consider the general solution,

$$\psi = a_1 e^{-i \frac{\omega(x, y)}{\mathcal{E}}} \psi_- + a_2 e^{i \frac{\omega(x, y)}{\mathcal{E}}} \psi_+, \quad (24)$$

with $\omega(x, y) = \int_0^x \varepsilon(x', y) dx'$. The coefficients a_1 and a_2 satisfy

$$\begin{aligned} \frac{\partial}{\partial x} a_1 &= -a_2 \mathcal{T}(x, y) - i a_1 \cos^2\left(\frac{\theta}{2}\right) \frac{\partial \phi}{\partial x} \\ \frac{\partial}{\partial x} a_2 &= -a_1 \mathcal{T}^*(x, y) - i a_2 \sin^2\left(\frac{\theta}{2}\right) \frac{\partial \phi}{\partial x}, \end{aligned} \quad (25)$$

with

$$\mathcal{T} = e^{2i \frac{\omega(x, y)}{\mathcal{E}}} \frac{iy(3x^2 - y^2) + x(x^2 - 3y^2)/\varepsilon(x, y)}{(x^2 + y^2)\varepsilon(x, y)}. \quad (26)$$

Now we take the adiabatic limit (i.e., we consider that the probability to undergo a transition from one adiabatic state to another is negligible, $a_2 \sim 1$). Then the transmission amplitude is

$$t(y) = \int_{-\infty}^{\infty} \mathcal{T}(x, y) dx. \quad (27)$$

In the limit $y \rightarrow 0$ this integral can be evaluated following the methods presented in Refs. 6,38 and we obtain (back in physical units) (see Appendix),

$$\begin{aligned} T(k_y, \tau_z) &\approx \frac{4\pi^2}{9} e^{-2c_1 \frac{M_0}{F} \frac{\sqrt{M_0 \gamma_1}}{\hbar v_F}} \sin^2 \left(c_1 \frac{M_0}{F} \frac{\sqrt{M_0 \gamma_1}}{\hbar v_F} \right) \\ &\times \left(1 - c_2 k_y \tau_z \left(\frac{F}{M_0} \right)^{1/3} \frac{(\hbar v_F)^{4/3}}{(M_0 \gamma_1)^{2/3}} \right), \end{aligned} \quad (28)$$

where $c_1 \approx 1.23$ and $c_2 \approx 3.19$ are numerical factors. Some comments on Eq. (28) are in order: (i) As shown in Fig. 3, there is reasonable agreement between the numerical results and the one obtained in the adiabatic approximation, (ii) the transition probability is not symmetric with respect to k_y , but it is so with respect to the product $k_y \tau_z$, (iii) the maximum transition occurs at finite k_y , (iv) there is an oscillatory term in the transmission amplitude that produces zeros in the tunneling probability at finite values of F , M_0 , and k_y . These zeros appear because the bilayer graphene Hamiltonian is quadratic in the momentum and, for each energy in the gap region, there are two decaying states that interfere under the tunneling barrier.²⁷

D. Trilayer graphene, diabatic basis, and sudden approximation

In ABC-stacked trilayer graphene the pseudospin unitary vector is

$$\vec{h}^t = \frac{\left(\frac{v_F^3}{\gamma_1^2} (4p_x^3 - 3p_x p^2), \frac{v_F^3}{\gamma_1^2} (3p^2 p_y - 4p_y^3) \tau_z, M_0 \right)}{\sqrt{M_0^2 + \frac{v_F^6}{\gamma_1^2} p^6}}. \quad (29)$$

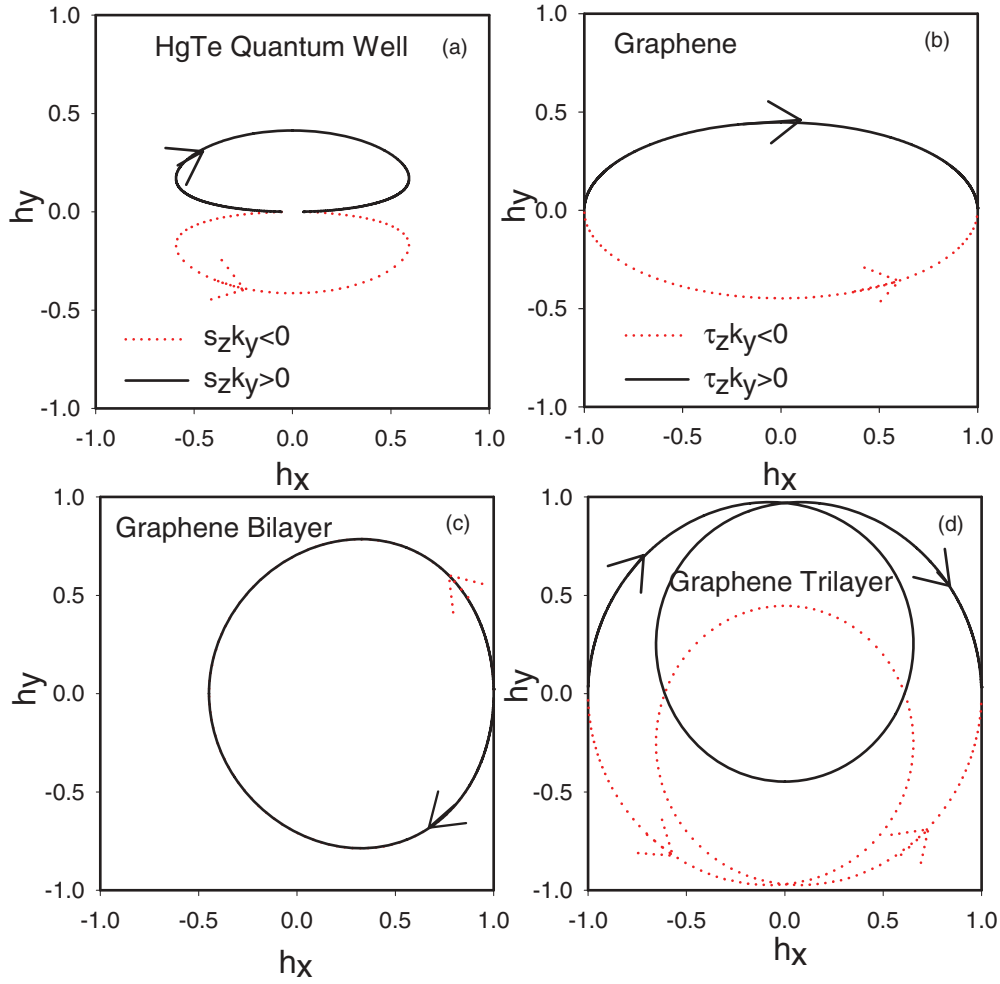


FIG. 4. (Color online) In-plane projection of the trajectory defined by the pseudospin $\vec{h}(\vec{k}_x, k_y)$ in an adiabatic reflection process. Solid lines correspond to trajectories with $s k_y > 0$ and dotted lines to trajectories with $s k_y < 0$.

For massless trilayer graphene the pseudospin reduces to $(4k_x^3 - 3k_x k^2, (3k_y k^2 - 4k_y^3)\tau_z, 0)/k^3$ and the eigenvectors are again chiral. Because the pseudospin rotates 6π when the wave vector rotates 2π around $\mathbf{k} = 0$, the transition probability at $k_y = 0$ is unity for massless trilayer graphene. In Fig. 2 we see that, even for $M_0 \neq 0$, in the limit of a large electric field the transition probability at small k_y is near one. Therefore, it is appropriate to work in the diabatic basis and use the sudden approximation. We write the Bloch equation as the sum of a diabatic term plus a perturbation,

$$i \frac{\partial}{\partial x} \psi = \frac{1}{\mathcal{E}} \left[\begin{pmatrix} 0 & x^3 \\ x^3 & 0 \end{pmatrix} + \begin{pmatrix} 1 & (x - i\tau_z y)^3 - x^3 \\ (x + i\tau_z y)^3 - x^3 & -1 \end{pmatrix} \right] \psi, \quad (30)$$

and in the case of the trilayer graphene we have

$$\mathcal{E} = \frac{M_0 (\gamma_1^2 M_0)^{1/3}}{F \hbar v_F}. \quad (31)$$

The eigenfunctions of the first term of Eq. (30) define the diabatic basis. In this basis the wave function takes the

form,

$$\psi(x) = \frac{C_-(x)}{\sqrt{2}} \begin{pmatrix} 1 \\ -1 \end{pmatrix} e^{i \frac{x^4}{4\mathcal{E}}} + \frac{C_+(x)}{\sqrt{2}} \begin{pmatrix} 1 \\ 1 \end{pmatrix} e^{-i \frac{x^4}{4\mathcal{E}}}, \quad (32)$$

and the coefficients C_- and C_+ satisfy

$$\partial_x C_{\mp} = \mp \frac{i}{\mathcal{E}} 3xy^2 C_{\pm} + \frac{i}{\mathcal{E}} (1 \pm iy\tau_z(y^2 - 3x^2)) e^{-i \frac{x^4}{4\mathcal{E}}} C_{\mp}. \quad (33)$$

To lowest order in $1/\mathcal{E}$ and y , the reflection amplitude is

$$r = C_- (+\infty) \simeq -\frac{i}{\mathcal{E}} \int_{-\infty}^{\infty} (1 - i3x^2 y \tau_z) e^{i \frac{x^4}{2\mathcal{E}}} dx \\ = \left(\frac{1}{\mathcal{E}}\right)^{3/4} \frac{\Gamma(1/4)}{2^{3/4}} e^{i \frac{3\pi}{8}} + \left(\frac{1}{\mathcal{E}}\right)^{1/4} 3\tau_z y \frac{\Gamma(3/4)}{2^{1/4}} e^{-i \frac{3\pi}{8}}, \quad (34)$$

and the transmission probability, in the physical units, is

$$T(k_y, \tau_z) = 1 - \frac{M_0^2 \gamma_1}{(\hbar v_F F)^{3/2}} \frac{\Gamma^2(1/4)}{2^{3/2}} \\ - \tau_z \frac{M_0 k_y}{F} \frac{\Gamma(1/4)\Gamma(3/4)}{\sqrt{2}}. \quad (35)$$

This expression agrees remarkably well with the numerical results for large electric fields (see Fig. 3). In addition, Eq. (35) explains qualitatively the dependence of the tunneling probability on the wave vector k_y .

V. BERRY PHASE AND LACK OF REFLECTION SYMMETRY

The question that remains is the physical origin of the asymmetry, for a fixed spin/valley, of the tunneling amplitude as a function of k_y . The asymmetry is not related to the Chern number associated with the chirality of the massless, $M_0 = 0$, Hamiltonians.³¹ Although HgTe and monolayer graphene share the same Chern number, in monolayer graphene the transition amplitude is symmetric with respect to k_y , whereas it is not so in HgTe quantum wells.

We associate the asymmetry with the winding of the expectation value of the pseudospin $\vec{h}(\mathbf{k})$ when a carrier is adiabatically reflected by the tunneling barrier. This is related to the sign of the Berry phase acquired by the carrier's pseudospin in this process.

Consider a quasiparticle moving in the valence band in the presence of a constant electric field, $V(x) = -Fx$. This quasihole coming from $x = -\infty$ and moving towards the right has a momentum $k_x < 0$. Upon arriving into the gapped region, it is adiabatically reflected from it back to $x = -\infty$ with momentum $k_x > 0$. In the presence of the electric field, the momentum k_x is not a good quantum number and it is not conserved. In a semiclassical/adiabatic approximation the momentum is defined by the relation,

$$\varepsilon(\vec{k}_x(x), k_y) - Fx = E. \quad (36)$$

eflection process the pseudospin $\vec{h}(\vec{k}_x, k_y)$ describes a trajectory on the Bloch sphere of radius unity. When the trajectory closes a circuit Γ in the unit sphere, the wave function of the carrier acquires a Berry phase equal to half the solid angle defined by the surface enclosed by the circuit Γ .

In Fig. 4 we plot, for the different Hamiltonians studied in this paper, the in-plane projection of the trajectories defined by the pseudospin \vec{h} when the carrier goes from $x = -\infty$ to the barrier and is reflected adiabatically back to $x = -\infty$. In the case of monolayer graphene such trajectory defines an open line, both for $\tau_z k_y$ greater or smaller than zero. Thus, for monolayer graphene there are no closed paths in the adiabatic process and there is no Berry phase associated with the reflection. The situation is different for HgTe quantum wells. In this case the trajectory defines a closed circuit and there is a Berry phase associated with the adiabatic reflection. The sign of the Berry phase depends on the direction in which the closed loop is traversed by the pseudospin. It turns out that it has an opposite sign for opposite signs of k_y or s_z . Therefore, the sign of the Berry phase depends on the sign of the product $k_y s_z$. For graphene multilayers, $N > 1$, the pseudospin trajectory in the adiabatic reflection process always defines closed paths that have opposite orientation for opposite values of the product $k_y \tau_z$. The dependence of the Berry phase on the product $k_y s$, being s the spin or the valley index, breaks the reflection symmetry in each index s and

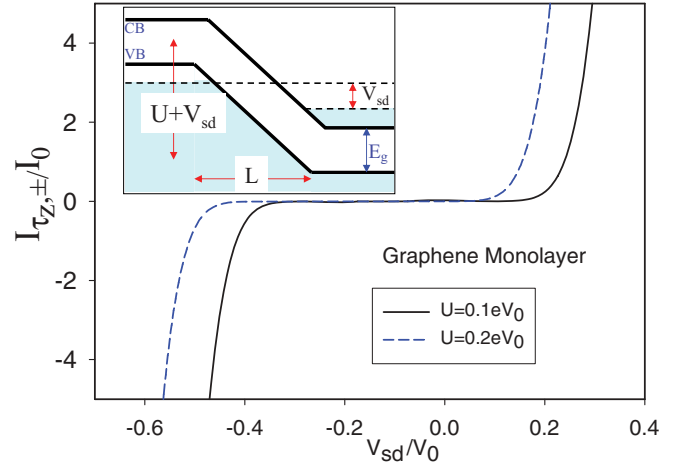


FIG. 5. (Color online) $I_{\tau_z, \pm} - V$ characteristics of monolayer graphene for two values of the built-in potential. Units are $I_0 = \frac{e^2}{h} V_0 W / d_M \times 10^6$ and $eV_0 = M_0 L / d_M$. The inset shows schematically the Zener diode.

explains the asymmetry of the transmission for a momentum k_y at a fixed index s .

VI. ZENER TUNNELING CURRENT

Finally, we calculate the tunneling current flowing through the Zener diode. We consider a p - n junction as the one

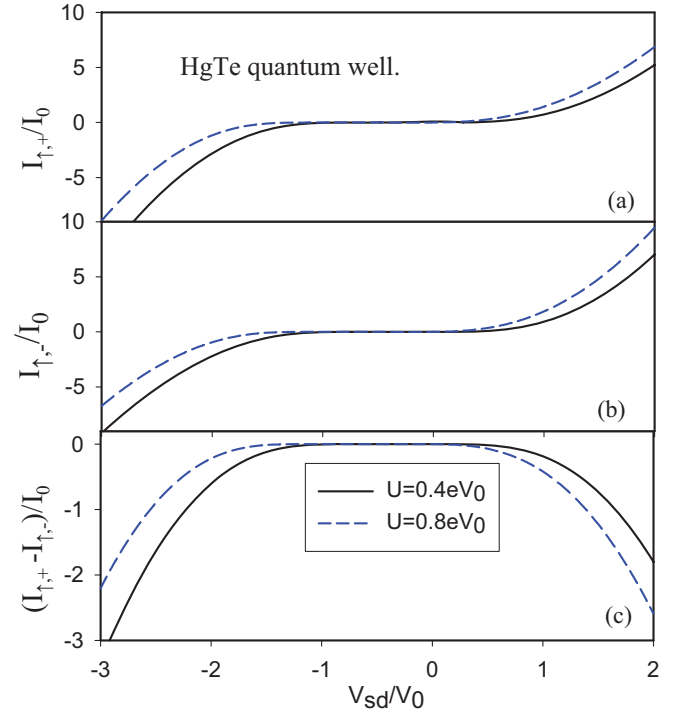


FIG. 6. (Color online) $I_{\tau_z, \pm} - V$ characteristics of HgTe quantum wells, for two values of the built-in potential. Panels (a) and (b) correspond to current flowing in the positive and negative \hat{y} direction, respectively. In panel (c) we plot the excess of current in the positive \hat{y} direction for electrons with spin-up. Units are $I_0 = \frac{e^2}{h} V_0 W / d_M \times 10^2$ and $eV_0 = M_0 L / d_M$.

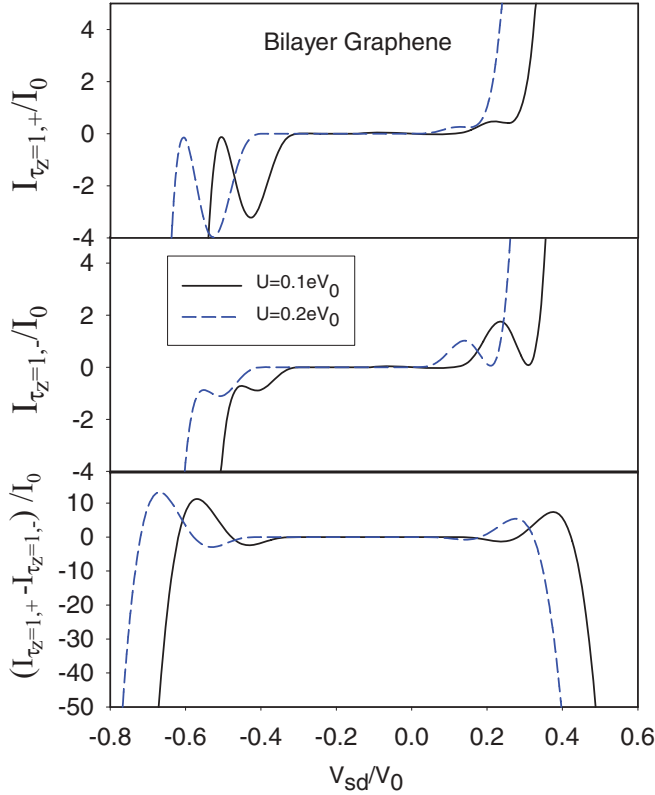


FIG. 7. (Color online) $I_{\tau_z=1,\pm}$ - V characteristics of bilayer graphene, for two values of the built-in potential. Panels (a) and (b) correspond to current flowing in the positive and negative \hat{y} direction, respectively. In panel (c) we plot the excess of current in the positive \hat{y} direction for electrons in the valley $\tau_z = 1$. Units are $I_0 = \frac{e^2}{h} V_0 W/d_M \times 10^5$ and $eV_0 = M_0$.

sketched in the inset of Fig. 5. U represents the built-in potential induced by doping or electrical gates, and V_{sd} is the source-drain potential difference. L is the junction length. Within the Landauer approximation, the tunneling current for index s moving in the positive \hat{y} direction has the form,

$$I_{s,+} = \frac{e}{h} \int_{-\infty}^{\infty} dE (n_{E-\frac{1}{2}eV_{sd}} - n_{E+\frac{1}{2}eV_{sd}}) \times \frac{W}{2\pi} \int_0^{q_y} T\left[k_y, s, \frac{e}{L}(U + V_{sd})\right] dk_y, \quad (37)$$

where n_E is the Fermi-Dirac distribution and W is the transverse length of the p - n interface. Although in the uniform field approximation the transition amplitude is energy independent, the limits of the integral in k_y depend on energy through the relation $E = \varepsilon(k_x = 0, q_y)$. The current flowing in the negative \hat{y} direction, $I_{s,-}$, is obtained performing the integral in k_y from $-q_y$ to 0. As the transition is dominated by small values of k_y (see Fig. 2 and Ref. 27), we approximate q_y by ∞ in the calculation of the currents. For zero temperature the current gets the form,

$$I_{s,\pm} = \pm \frac{e^2}{h} V_{sd} \frac{W}{2\pi} \int_0^{\pm\infty} T\left[k_y, s, \frac{e}{L}(U + V_{sd})\right] dk_y. \quad (38)$$

This current verifies the symmetries $I_{s,+} = I_{-s,-}$ and $I_{s,-} = I_{-s,+}$.

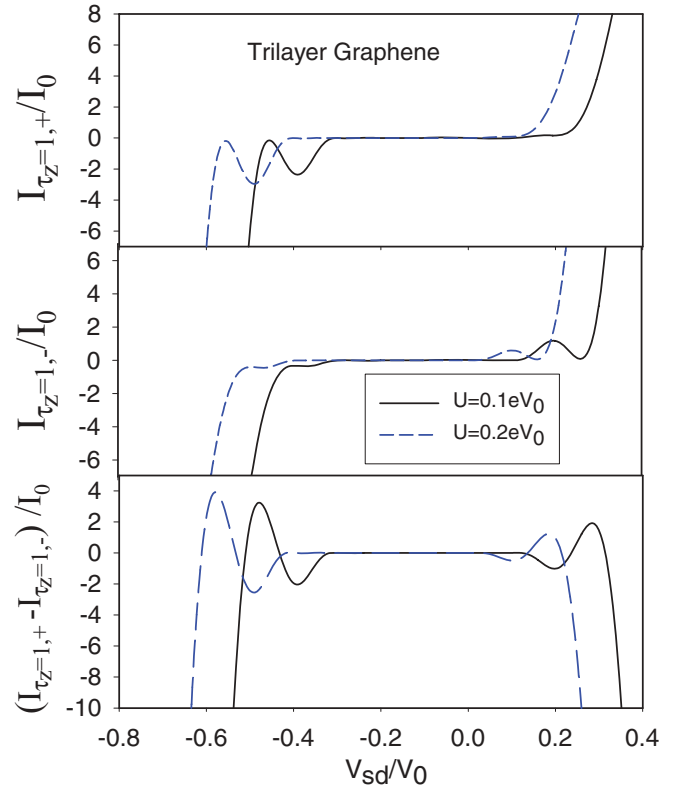


FIG. 8. (Color online) $I_{\tau_z=1,\pm}$ - V characteristics of trilayer graphene, for two values of the built-in potential. Panels (a) and (b) correspond to current flowing in the positive and negative \hat{y} direction, respectively. In panel (c) we plot the excess of current in the positive \hat{y} direction for electrons in the valley $\tau_z = 1$. Units are $I_0 = \frac{e^2}{h} V_0 W/d_M \times 10^4$ and $eV_0 = M_0$.

In Fig. 5 we plot the $I_{\tau_z,\pm 1}$ - V characteristics for monolayer graphene and different values of U . The curves present the breakdown-type behavior characteristic of a Zener diode. In the case of monolayer graphene the transmission amplitude is symmetric with respect to the momentum k_y and the current is equal for positive and negative \hat{y} direction.

In Fig. 6 we plot the $I_{\uparrow,\pm 1}$ - V curves for a HgTe quantum well and different values of U . For spin-up there is an excess of current in the negative \hat{y} direction. This effect is the opposite for spin-down electrons. These results indicate the existence of a spin current perpendicular to the Zener barrier. This Zener tunneling spin Hall effect is a consequence of the asymmetry in the transition curves of Fig. 2. From Fig. 6 we obtain that the Hall spin current can be as large as 30% of the electrical current. Because a HgTe quantum well may be a two-dimensional topological insulator under certain conditions, there is an extra contribution to the current in this case coming from the spin-polarized edge states developed in the barrier region. However, its magnitude is always of the order of one conductance quantum $\sim e^2/h$ or less, since the electric field diminishes it.³⁹ On the other hand, the Zener tunneling spin Hall current is proportional to the transverse length W [see Eq. (38)] and increases with the electric field.

In Figs. 7 and 8 we plot the I - V characteristic curves for bilayer- and trilayer-based Zener diodes. In both cases there are some oscillations on top of the nonlinear, N-shaped I - V

curves. These negative differential conductivities appear for positive and negative \hat{y} directions, and they have their origin in the interference between decaying states in the energy gap region.²⁷ In trilayer graphene the negative differential conductivity is even stronger than in bilayer graphene. At large source-to-drain voltage, the asymmetry of the tunneling amplitude is reflected in an excess of current in the negative \hat{y} direction with respect to the positive \hat{y} direction. For multilayer graphene, this effect is the opposite depending on the valley τ_z . These results indicate the existence of a valley current perpendicular to the Zener barrier that is a consequence of the asymmetry in the transition curves of Fig. 2.

VII. SUMMARY

We have analyzed Zener diode physics in HgTe quantum wells and multilayer graphene. In the case of HgTe quantum wells we find that, after traversing the barrier, a Zener tunneling spin Hall current is developed to the right of the diode. In the case of bilayer and trilayer graphene the Zener diode generates a valley Hall current. This effect is absent for the monolayer graphene. The magnitude and polarization of the Hall currents increase with the applied electric field.

The tunneling current is obtained from the transmission probability that is computed numerically in the constant electric field approximation. The origin of the Hall currents is the asymmetry of the transmission probability in the momentum k_y perpendicular to the tunneling barrier. We have developed an analytical approximation for the tunneling transmission at small k_y that agrees rather well with the numerical results. The physical origin of the Zener tunneling asymmetry on k_y is related to the Berry phase that the carriers acquire when they are adiabatically reflected from the tunneling region.

In the case of multilayer graphene the Zener tunneling valley Hall effect could be used for valleytronic applications.^{40,41} In an appropriated geometry, the asymmetry in the Zener tunneling should enable one to spatially separate the carriers of each valley⁴², which could be useful to manipulate the valley degree of freedom in bulk graphene.

The Zener tunneling spin Hall effect we predict to occur in HgTe quantum wells could be used for electrical manipulation of the spin currents. The spin currents in the Zener device

should be stronger than those occurring in diffusive systems, and they could be detected in nonlocal electrical measurements in H-shaped structures.⁴³

ACKNOWLEDGMENTS

We acknowledge fruitful discussions with B. Dóra, S. Kohler, and M. O. Goerbig. Funding for this work was provided by MICINN-Spain via Grant No. FIS2009-08744, the CSIC JAE-Doc program, and was supported in part by the National Science Foundation under Grant No. NSF PHY05-51164.

APPENDIX

In this appendix we evaluate the integral of Eq. (27). In the limit $y \rightarrow 0$, the transition probability takes the form,

$$t = \int_{-\infty}^{\infty} dx e^{-i2\frac{\omega(x,y=0)}{\varepsilon}} \left(\frac{x}{1+x^4} + i \frac{3y}{\sqrt{1+x^4}} \right). \quad (\text{A1})$$

In terms of $\omega(x, y=0)$, the integral has simple poles in the complex plane at $\omega_i = \int_0^{x_i} dx \sqrt{1+x^4}$, where $x_i = \pm e^{\pm i\pi/4}$. Expanding the value of ω near x_i we find

$$\omega(x, y=0) - \omega_i \simeq \frac{4}{3} x_i^{3/2} (x - x_i)^{3/2}, \quad (\text{A2})$$

and we rewrite

$$\begin{aligned} t &= \int_{-\infty}^{\infty} d\omega e^{-i2\frac{\omega}{\varepsilon}} \left(\frac{x(\omega)}{(d\omega/dx)^3} + \frac{3iy}{(d\omega/dx)^2} \right) \\ &= \sum_i \int_{-\infty}^{\infty} d\omega e^{-i2\frac{\omega}{\varepsilon}} \left(\frac{x(\omega)}{6(\omega - \omega_i)x_i^3} \right. \\ &\quad \left. + \frac{3iy}{6^{2/3}(\omega - \omega_i)^{2/3}x_i^2} \right). \end{aligned} \quad (\text{A3})$$

We solve this integral by closing the path around the lower half of the complex plane. This path encloses the poles $\sqrt{2}/2(\pm 1, -i)$ and their associated branches. The integral then yields

$$t(y) = i \frac{2\pi}{3} e^{-c_1 \frac{1}{\varepsilon}} \sin \left(c_1 \frac{1}{\varepsilon} \right) (1 - c_2 \varepsilon^{1/3} y), \quad (\text{A4})$$

with $c_1 = \frac{1}{4} \sqrt{\frac{\pi}{2}} \frac{\Gamma(1/4)}{\Gamma(7/4)}$ and $c_2 = \frac{3^{4/3}}{\Gamma(2/3)}$.

¹S. M. Sze, *Physics of Semiconductor Devices* (Wiley, New York, 1981).

²C. Zener, *Proc. Royal Soc. London* **145**, 523 (1934).

³C. Wittig, *J. Phys. Chem. B* **109**, 8428 (2005).

⁴E. O. Kane and E. Blount, *Tunneling Phenomena in Solids* (Plenum Press, New York, 1969).

⁵S. N. Shevchenko, S. Adshab, and F. Nori, *Phys. Rep.* **492**, 1 (2010).

⁶E. Shimshoni and Y. Gefel, *Ann. Phys.* **201**, 16 (1991).

⁷X.-L. Qi *et al.*, *Phys. Rev. B* **74**, 085308 (2006).

⁸B. Bernevig *et al.*, *Science* **314**, 1757 (2006).

⁹M. König *et al.*, *Science* **318**, 766 (2007).

¹⁰L. Fu *et al.*, *Phys. Rev. Lett.* **98**, 106803 (2007).

¹¹J. E. Moore *et al.*, *Phys. Rev. B* **75**, 121306 (2007).

¹²S. Murakami, *New J. Phys.* **9**, 356 (2007).

¹³K. S. Novoselov, A. K. Geim, S. V. Morozov, D. Jiang, Y. Zhang, S. V. Dubonos, I. V. Gregorieva, and A. A. Firsov, *Science* **306**, 666 (2004).

¹⁴K. S. Novoselov, D. Jiang, T. Booth, V. V. Khotkevich, S. M. Morozov, and A. K. Geim, *Nature (London)* **438**, 197 (2005).

¹⁵Y. Zhang, Y.-W. Tan, H. L. Stormer, and P. Kim, *Nature (London)* **438**, 201 (2005).

- ¹⁶M. I. Katsnelson, K. S. Novoselov, and A. Geim, *Nat. Phys.* **2**, 620 (2006).
- ¹⁷V. V. Cheianov and V. I. Fal'ko, *Phys. Rev. B* **74**, 041403 (2006).
- ¹⁸J. R. Williams, L. DiCarlo, and C. M. Marcus, *Science* **317**, 638 (2007).
- ¹⁹L. M. Zhang and M. M. Fogler, *Phys. Rev. Lett.* **100**, 116804 (2008).
- ²⁰A. Young and P. Kim, *Nat. Phys.* **5**, 222 (2009).
- ²¹N. Vandecasteele, A. Barreiro, M. Lazzeri, A. Bachtold, and F. Mauri, *Phys. Rev. B* **82**, 045416 (2010).
- ²²N. Stander, B. Huard, and D. Goldhaber-Gordon, *Phys. Rev. Lett.* **102**, 026807 (2009).
- ²³D. Jena, T. Fang, Q. Zhang, and H. Xing, *Appl. Phys. Lett.* **93**, 112106 (2008).
- ²⁴H.-Y. Chiu, V. Perebeinos, Y.-M. Lin, and P. Avouris, *Nano Lett.* **10**, 4634 (2010).
- ²⁵L. Brey and H. A. Fertig, *Phys. Rev. Lett.* **103**, 046809 (2009).
- ²⁶D. P. Arovas, L. Brey, H. A. Fertig, E.-A. Kim, and K. Ziegler, *New J. Phys.* **12**, 123020 (2010).
- ²⁷R. Nandkishore and L. Levitov, *Proceedings of the National Academy of Sciences* **108**, 14021 (2011).
- ²⁸Typical parameters for HgTe quantum wells are⁴⁴ $M_0 \sim 10$ meV, $B \sim 1.2$ eV nm², $A \sim 0.38$ eV nm.
- ²⁹C. L. Kane and E. J. Mele, *Phys. Rev. Lett.* **95**, 226801 (2005).
- ³⁰C. L. Kane and E. J. Mele, *Phys. Rev. Lett.* **95**, 146802 (2005).
- ³¹E. Prada, P. San-Jose, L. Brey, and H. Fertig, *Solid State Commun.* **151**, 1075 (2011).
- ³²A. H. Castro-Neto, F. Guinea, N. M. R. Peres, K. S. Novoselov, and A. K. Geim, *Rev. Mod. Phys.* **81**, 109 (2009).
- ³³H. Min, G. Borghi, M. Polini, and A. H. MacDonald, *Phys. Rev. B* **77**, 041407 (2008).
- ³⁴E. McCann, D. S. Abergel, and V. I. Fal'ko, *Solid State Commun.* **143**, 110 (2007).
- ³⁵M. Z. Hasan and C. L. Kane, *Rev. Mod. Phys.* **82**, 3045 (2010).
- ³⁶X.-L. Qi and S.-C. Zhang, *Rev. Mod. Phys.* **83**, 1057 (2011).
- ³⁷M. Guigou, P. Recher, J. Cayssol, and B. Trauzettel, *Phys. Rev. B* **84**, 094534 (2011).
- ³⁸J. Davis and P. Pechukas, *J. Chem. Phys.* **64**, 3129 (1976).
- ³⁹B. Dóra and R. Moessner, *Phys. Rev. B* **83**, 073403 (2011).
- ⁴⁰A. Rycerz, J. Tworzydło, and C. W. J. Beenakker, *Nature Physics* **3**, 172 (2007).
- ⁴¹D. Xiao, W. Yao, and Q. Niu, *Phys. Rev. Lett.* **99**, 236809 (2007).
- ⁴²H. Schomerus, *Phys. Rev. B* **82**, 165409 (2010).
- ⁴³C. Brune *et al.*, *Nat. Phys.* **6**, 448 (2010).
- ⁴⁴G. Tkachov *et al.*, *Phys. Rev. Lett.* **106**, 076802 (2011).